

PatchScaler: An Efficient Patch-Independent Diffusion Model for Image Super-Resolution

Yong Liu^{1,2} Hang Dong^{3*} Jinshan Pan⁴ Qingji Dong^{1,2} Kai Chen³
Rongxiang Zhang³ Lean Fu³ Fei Wang^{1,2}
¹National Key Laboratory of Human-Machine Hybrid Augmented Intelligence
²IAIR, Xi'an Jiaotong University ³ByteDance Inc
⁴Nanjing University of Science and Technology

Abstract

While diffusion models significantly improve the perceptual quality of super-resolved images, they usually require a large number of sampling steps, resulting in high computational costs and long inference times. Recent efforts have explored reasonable acceleration schemes by reducing the number of sampling steps. However, these approaches treat all regions of the image equally, overlooking the fact that regions with varying levels of reconstruction difficulty require different sampling steps. To address this limitation, we propose PatchScaler, an efficient patch-independent diffusion pipeline for single image super-resolution. Specifically, PatchScaler introduces a Patch-adaptive Group Sampling (PGS) strategy that groups feature patches by quantifying their reconstruction difficulty and establishes shortcut paths with different sampling configurations for each group. To further optimize the patch-level reconstruction process of PGS, we propose a texture prompt that provides rich texture conditional information to the diffusion model. The texture prompt adaptively retrieves texture priors for the target patch from a common reference texture memory. Extensive experiments show that our PatchScaler achieves superior performance in both quantitative and qualitative evaluations, while significantly speeding up inference. Our code will be available at <https://github.com/yongliu/PatchScaler>.

1. Introduction

Single image super-resolution (SISR) aims to reconstruct a high-resolution (HR) image from its low-resolution (LR) observation, a highly ill-posed problem due to the unknown degradation processes in real-world scenarios. As two predominant approaches, deep convolutional neural network (CNN)-based [23, 49, 65, 69] and Transformer-based [25, 27, 55, 66] SISR methods have made significant

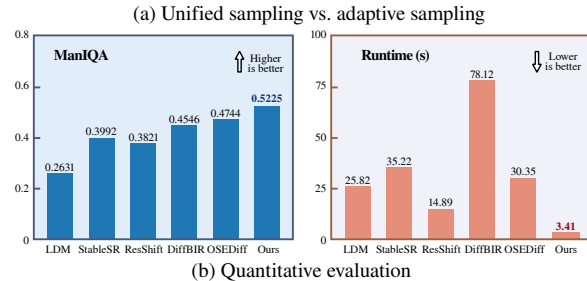
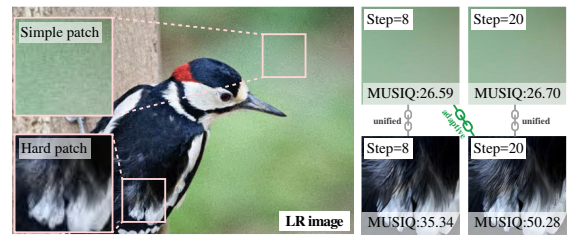


Figure 1. (a) Qualitative analysis of unified sampling and adaptive sampling. (b) Quantitative comparison of diffusion-based SR methods on RealSR [6] dataset. Noted that the runtime is measured on the $\times 4$ (512 \rightarrow 2048) SR task using an NVIDIA Tesla A100 GPU.

progress in the past decade. However, most of them are optimized primarily for the peak signal-to-noise ratio (PSNR) and the structural similarity index measure (SSIM), which are less effective in restoring realistic image details.

Diffusion models [12, 41], with their powerful ability to model data distributions from noise, have offered immense potential for conditional generation tasks, such as image synthesis [9, 38, 56], image editing [5, 16, 54], and image super-resolution [26, 45, 59]. Although diffusion models have achieved significant success in the field of image super-resolution (SR), their inference process remains inefficient due to the large number of iterative sampling steps required for high-quality image reconstruction.

Recent methods have attempted to accelerate diffusion-based SR models by introducing conditional distillation [31, 50] or redefining the diffusion process [61, 62]. However, these approaches tend to treat all regions of an im-

*Corresponding author.

age equally and indiscriminately reduce the number of sampling steps, which inevitably compromises the quality of the super-resolved images. Furthermore, when dealing with high-resolution images, these approaches continue to incur substantial computational costs.

In this paper, we observe that a unified sampling process is suboptimal for all patches of an image. As illustrated in Figure 1 (a), patches with fewer structural details can be effectively reconstructed with fewer sampling steps, whereas patches rich in textural information require more sampling steps. This observation motivates us to develop a patch-adaptive accelerated diffusion model for SISR.

Based on this insight, we propose PatchScaler, an efficient diffusion-based SR method that dynamically accelerates the inference process through an adaptive, patch-independent diffusion pipeline. Specifically, we first employ a global restoration module to generate a coarse HR feature along with a confidence map that reflects the reconstruction difficulty across different regions. We then introduce Patch-adaptive Group Sampling (PGS), which divides the coarse HR features into patches and groups them according to quantified reconstruction difficulty. PGS identifies an optimal intermediate point and sampling configurations for each group, enabling a shortcut path from coarse HR patches to the ground truths. Finally, we introduce a Patch-wise Diffusion Transformer (Patch-DiT) as the backbone of PatchScaler to refine the fine textures from the coarse HR patches. Since the reconstruction of local image textures plays a more critical role for SISR than the Text2Image task, Patch-DiT is naturally well-suited for restoring lost details.

To further optimize the patch-level reconstruction process of PGS, we propose a texture prompt that supplies rich conditional information to Patch-DiT by retrieving high-quality texture priors for the target patch from a universal reference texture memory. The texture prompt is effective for reconstructing local details and addressing the misalignment issue between image and text prompts in diffusion models [7]. Experiments show that our PatchScaler significantly accelerates inference speed (e.g., only $0.23\times$ the runtime of ResShift [62] on the $512\rightarrow 2048$ SR task), while still maintaining superior performance, as shown in Figure 1(b). We summarize our main contributions as follows:

- We propose PatchScaler, a novel patch-independent SR pipeline that employs patch-adaptive group sampling to dynamically accelerate the sampling process, enabling efficient restoration of high-resolution images.
- We present an effective texture prompt for the Patch-wise Diffusion Transformer (Patch-DiT) in PatchScaler to provide rich texture priors and improve reconstruction quality.
- Experiments show that PatchScaler achieves favorable performance on several datasets against state-of-the-art SR methods and is much more efficient than previous diffusion-based SR methods.

2. Related Work

Single Image Super-Resolution. Over the past decade, a series of deep networks [21, 27, 33, 42, 69] have been proposed to address SISR challenges. For real-world degradation scenarios, Ji *et al.* [13] proposed RealSR that learns the specific degradation of blurry and noisy images by estimating the kernel and noise. By incorporating GANs [10, 40, 48] into the SISR task, Zhang *et al.* [63] presented BSRGAN, a practical degradation model that synthesizes realistic degradations via a random shuffling strategy. Wang *et al.* [49] proposed Real-ESRGAN that employs a high-order degradation process to simulate practical degradations and incorporates sinc filters to replicate common ringing and overshoot artifacts. Liang *et al.* [25] introduced SwinIR-GAN based on the Swin Transformer [28], to achieve competitive image restoration performance. Nevertheless, these approaches often struggle to generate realistic fine details.

Diffusion Model. The powerful generative capabilities inherent in diffusion models have yielded remarkable performance in SISR task. Specifically, Wang *et al.* [45] presented StableSR, integrating LR images into diffusion models via a time-aware encoder to reconstruct high-quality HR images. Lin *et al.* [26] proposed a unified restoration framework DiffBIR, which sequentially uses two stages of restoration and generation to ensure fidelity and realism. Yue *et al.* [62] introduced ResShift, utilizing a novel iterative sampling approach from LR to HR images by shifting residuals. Although these approaches have achieved considerable improvements in perceptual quality, they treat all regions of an image equally and indiscriminately adopt a unified sampling strategy during inference, even for easily restored patches. In contrast, our work explores a more efficient patch-independent diffusion pipeline, achieving superior results with faster inference speed.

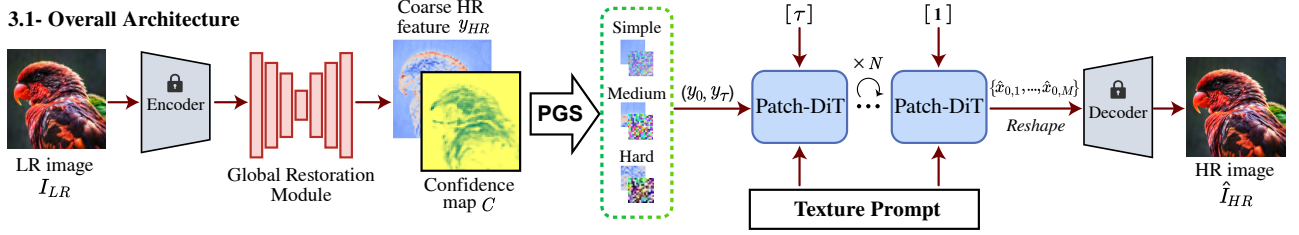
3. Proposed Method

3.1. Overall Architecture

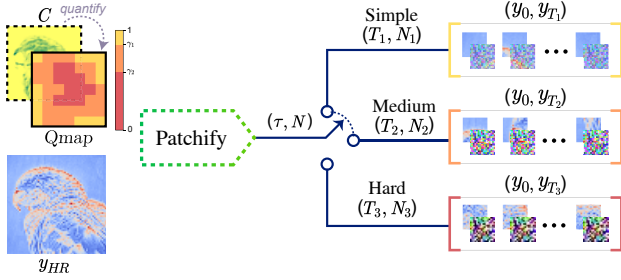
The overall architecture of PatchScaler is illustrated in Figure 2. Given an LR image $I_{LR} \in \mathbb{R}^{3 \times H \times W}$, we first encode it into a latent representation $\mathbf{y}_{LR} \in \mathbb{R}^{c \times \frac{H}{d} \times \frac{W}{d}}$ through the frozen encoder of the autoencoder, where d is the downsampling factor. Next, we employ a Global Restoration Module (GRM) to remove the degradations (e.g., noise or distortion artifacts) and capture long-range dependencies in \mathbf{y}_{LR} . To assess the reconstruction difficulty of different regions, a coarse HR feature $\mathbf{y}_{HR} \in \mathbb{R}^{c \times \frac{H}{d} \times \frac{W}{d}}$ and a corresponding confidence map $C \in \mathbb{R}^{1 \times \frac{H}{d} \times \frac{W}{d}}$ are simultaneously generated by GRM. Thus, we incorporate the confidence-driven loss [33] as a constraint and the training objective is:

$$L(\theta) := \|\mathbf{y}_{HR} - \mathbf{x}_{HR}\|_1^2 + \lambda(C \|\mathbf{y}_{HR} - \mathbf{x}_{HR}\|_2^2 - \eta \log(C)). \quad (1)$$

3.1- Overall Architecture



3.2- Patch-adaptive Group Sampling (PGS)



3.3- Texture Prompt

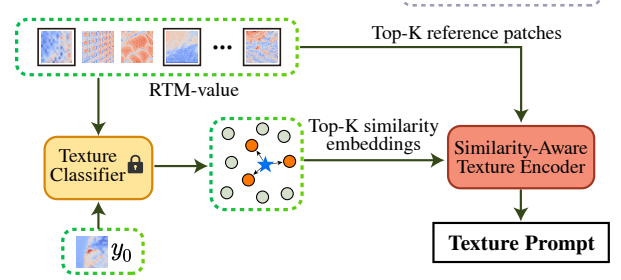


Figure 2. Overview of the proposed PatchScaler. PGS dynamically assign feature patches into groups with different sampling configuration based on quantified confidence map. Moreover, the texture prompt provides high-quality conditional information for Patch-DiT by retrieving high-quality texture priors from universal RTM.

Before initiating the diffusion process, we introduce Patch-adaptive Group Sampling (PGS), which dynamically divides \mathbf{y}_{HR} into patches grouped according to their reconstruction difficulties. Specifically, PGS partitions \mathbf{y}_{HR} into a patch set $\{\mathbf{y}_{0,1}, \mathbf{y}_{0,2}, \dots, \mathbf{y}_{0,M}\}$, where $\mathbf{y}_{0,i} \in \mathbb{R}^{c \times V \times V}$, with V and M denote the size of each patch and the length of the patch set, respectively. To define the reconstruction difficulty of $\mathbf{y}_{0,i}$, a quantified confidence map $Qmap$ is generated by averaging the confidence map C within the patch:

$$Qmap_{\mathbf{y}_{0,i}} := \begin{cases} \text{Simple,} & Avg(C \langle \mathbf{y}_{0,i} \rangle) \in (\gamma_1, 1], \\ \text{Medium,} & Avg(C \langle \mathbf{y}_{0,i} \rangle) \in (\gamma_2, \gamma_1], \\ \text{Hard,} & Avg(C \langle \mathbf{y}_{0,i} \rangle) \in [0, \gamma_2] \end{cases} \quad (2)$$

where $Avg(C \langle \mathbf{y}_{0,i} \rangle)$ represents the average confidence value over the patch, γ_1 and γ_2 are the confidence thresholds. Based on the resulting $Qmap$, PGS classifies the patches into different groups (i.e., "simple", "medium", and "hard") and assigns optimized sampling configurations during the subsequent diffusion process. Figure 3 presents two examples of coarse HR images generated by GRM along with the corresponding quantified confidence maps $Qmap$ calculated by Equation (2). It can be seen that our method accurately quantifies the reconstruction difficulty of different regions within the image. Patches with complex textures are assigned to the "hard" group, while relatively smooth patches are categorized as the "simple" group. In this way, PGS provides additional flexibility in handling various feature regions, thus significantly accelerating the inference process.

Since most popular open-source diffusion models [32, 38, 39] produce inferior results in low-resolution patches [68],

we build the diffusion backbone, Patch-DiT, based on DiTs[34]. Due to the inherent token sequence designation of Transformer, Patch-DiT is well-suited to handle patch-level features. Furthermore, we introduce a novel texture prompt as a conditional input for Patch-DiT to enhance its texture generation capabilities. The texture prompt provides rich texture priors by retrieving high-quality texture patches from a universal reference texture memory.

Finally, the HR patch set $\{\hat{\mathbf{x}}_{0,1}, \hat{\mathbf{x}}_{0,2}, \dots, \hat{\mathbf{x}}_{0,M}\}$ generated by Patch-DiT is reshaped into $\hat{\mathbf{x}}_{HR} \in \mathbb{R}^{4 \times \frac{H}{d} \times \frac{W}{d}}$ and passed to the decoder to obtain the HR output $\hat{\mathbf{I}}_{HR}$.

3.2. Patch-adaptive Group Sampling

Existing text-to-image models, such as Denoising Diffusion Probabilistic Models (DDPM) [12, 41], assume a forward diffusion trajectory where Gaussian noise is gradually applied to real data \mathbf{x}_0 :

$$q(\mathbf{x}_t | \mathbf{x}_{t-1}) = \mathcal{N}(\mathbf{x}_t; \sqrt{1 - \beta_t} \mathbf{x}_{t-1}, \beta_t \mathbf{I}), \quad (3)$$

where $t = 1, \dots, T$ and \mathbf{x}_t is the variable at time step t . The noise schedule $\{\beta_t\}$ can either be predefined or learned. Using the reparameterization trick, this process can be expressed in a closed form as:

$$q(\mathbf{x}_t | \mathbf{x}_0) = \mathcal{N}(\mathbf{x}_t; \sqrt{\bar{\alpha}_t} \mathbf{x}_0, (1 - \bar{\alpha}_t) \mathbf{I}), \quad (4)$$

where $\alpha_t := 1 - \beta_t$ and $\bar{\alpha}_t := \prod_{i=0}^t \alpha_i$. \mathbf{x}_t can be sampled by $\mathbf{x}_t = \sqrt{\bar{\alpha}_t} \mathbf{x}_0 + \sqrt{(1 - \bar{\alpha}_t)} \epsilon$ for $\epsilon \sim \mathcal{N}(0, \mathbf{I})$. In the reverse process, denoising models $f_\theta(\mathbf{x}_t, t)$ are trained to map any point at any time step on the diffusion trajectory to the starting point \mathbf{x}_0 .

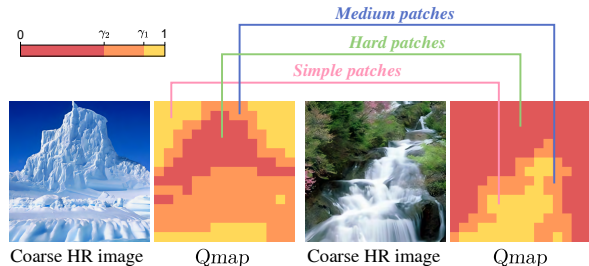


Figure 3. Examples of coarse HR images and corresponding $Qmap$. Our approach can accurately quantify the reconstruction difficulty of different regions across diverse scenes.

However, when these diffusion models are applied to SISR, there is a deviation between the LR image and the ground truth. To obtain a reasonable initial point for the reverse denoising process, previous approaches either apply a large noise strength (*i.e.*, $t = T$) to the LR image, approximating the endpoint x_T of diffusion trajectory, or sample x_T directly from a Gaussian noise $\mathcal{N}(0, \mathbf{I})$. Subsequently, the HR result is reconstructed step by step from x_T with a unified global sampling that treats all regions of the image equally. However, we argue that it is redundant because simple patches can be reconstructed with fewer iterations than hard patches, as illustrated in Figure 1(a). To enable dynamic acceleration of the denoising process, we propose Patch-adaptive Group Sampling (PGS), which establishes a shortcut path between HR patch x_0 and coarse HR patch y_0 , as shown in Figure 4. Here, y_0 is taken from the patch set.

Specifically, let $x_0 = y_0 + \Delta x_0$, then Equation (4) can be reformulated as:

$$q(x_t | y_0, \Delta x_0) = \mathcal{N}(x_t; \sqrt{\bar{\alpha}_t}(y_0 + \Delta x_0), (1 - \bar{\alpha}_t) \mathbf{I}). \quad (5)$$

The goal of PGS is to identify an appropriate intermediate point along the diffusion trajectory for each patch based on the distance Δx_0 . Since the GRM has removed the degradation (such as noise and distortion artifacts) from the LR input, Δx_0 is relatively small, especially for patches with fewer structural details. Therefore, an appropriate intermediate time step $\tau \in [1, T]$ can be determined such that $\sqrt{\bar{\alpha}_\tau} \Delta x_0 \rightarrow 0$. For small Δx_0 , τ can be small enough, while for a larger values Δx_0 , a larger τ is required to ensure that $\bar{\alpha}_\tau$ is sufficiently small. In this way, we can approximate the original diffusion trajectory at time step τ as:

$$q(x_\tau | y_0) \approx \mathcal{N}(x_\tau; \sqrt{\bar{\alpha}_\tau} y_0, (1 - \bar{\alpha}_\tau) \mathbf{I}). \quad (6)$$

This finding encourages us to introduce a new forward diffusion trajectory for the coarse HR patch y_0 with truncated forward diffusion time steps:

$$q(y_t | y_0) = \mathcal{N}(y_t; \sqrt{\bar{\alpha}_t} y_0, (1 - \bar{\alpha}_t) \mathbf{I}), \quad (7)$$

where $t = 1, \dots, \tau$. As a result, the reverse process can start from a non-Gaussian distribution y_τ that has a shorter

Algorithm 1 Retrieval Texture Priors from RTM.

Input: \mathcal{T} ; RTM-key; RTM-value; y_0

$\triangleright \mathcal{T}$ represents the feature extraction module of Texture Classifier; RTM-key=Normalize(\mathcal{T} (RTM-value)).

- 1: Obtain corresponding semantic feature vector from y_0 : $y\text{-query} = \mathcal{T}(y_0)$;
- 2: Calculate normalized inner products between $y_0\text{-query}$ and RTM-key $_i$:
 $s_i = \langle \text{RTM-key}_i, \text{Normalize}(y_0\text{-query}) \rangle$;
- 3: Ranking s_i and determine top-K indexes d^k and top-K similarities s^k ;
- 4: Retrieve corresponding texture prior tp^k from RTM-value based on top-K indexes d^k ;

Output: Texture prior tp^k ; top-K similarities s^k .

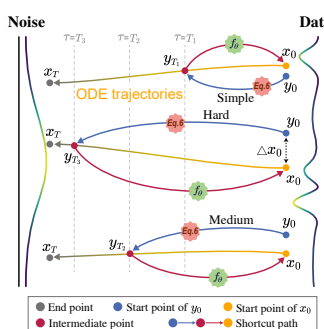


Figure 4. Illustration of the proposed PGS, which establishes a shortcut path between x_0 and y_0 . PGS treats different patches discriminatively and dynamically assign different sampling configurations. Here, y_0 and x_0 denote the coarse HR patch and ground truth, respectively. f_θ denotes the diffusion model Patch-DiT.

distance to x_0 , thus significantly reducing the required number of sampling steps N . This allows PGS to discriminatively handle feature patches with varying reconstruction difficulties, thereby increasing the flexibility of the reverse denoising process.

In practice, Δx_0 is estimated based on the confidence map C as the ground truth x_0 is unavailable during inference. To facilitate parallel computing and improve efficiency, we derive the quantified confidence map $Qmap$ from C using Equation (2) and divide the coarse HR feature patches into three groups (*i.e.*, simple, medium, and hard), as shown in the bottom-left part of Figure 2. Furthermore, we set different intermediate time steps $T_1 < T_2 < T_3$ and sampling steps $N_1 < N_2 < N_3$ for patches belonging to "simple", "medium", and "hard" groups, respectively. By assigning different sampling configurations to each group, PatchScaler can dynamically accelerate the sampling process.

3.3. Texture Prompt

To optimize the patch-level reconstruction process of PGS, we propose a texture prompt inspired by the reference SR [36, 53, 67], which provides rich conditional information for Patch-DiT. The texture prompt retrieves highly correlated texture priors from a Reference Texture Memory (RTM) and transfers them into the mainstream of Patch-DiT, as illustrated in the bottom-right part of Figure 2.

Reference Texture Memory. Our RTM serves as a repository for storing diverse and high-quality texture feature patches (denoted as *RTM-value*), along with their corresponding semantic feature vectors (denoted as *RTM-key*), to provide universal texture priors for Patch-DiT. To construct the RTM, we first extract 20,000 initial latent texture patches (i.e., *RTM-value*) from the high-quality image datasets DIV2K [1], OutdoorSceneTraining [47], and Manga109 [30], which contain a wide variety of categories, such as animal, sky, cartoon, building, mountain, and plant. Subsequently, we introduce a pre-trained Texture Classifier to extract deep semantic representation (i.e., *RTM-key*) from the initial *RTM-value*. To accelerate the feature retrieval process, we employ the farthest point sampling algorithm [35] on both *RTM-value* and *RTM-key* to sample the final 2,000 representative pairs, which form our final RTM. It is important to note that all of these operations are performed offline, thus incurring no additional inference cost.

Texture Retrieval and Transfer. Our objective is to retrieve high-quality texture priors with semantic similarity to the target feature patch y_0 from RTM and transfer them into Patch-DiT as a texture prompt. To achieve this, we first use the texture classifier to project y_0 into a semantic feature vector, denoted as y_0 -query. We then calculate the similarity scores between y_0 -query and *RTM-key* using normalized inner products [67]. By ranking these similarity scores, we retrieve the top- K matches, denoted as d^k , along with corresponding texture prior tp^k , for y_0 -query across the entire *RTM-key*. The complete retrieval process is shown in Algorithm 1. Subsequently, we integrate a similarity-aware texture encoder to transfer texture priors into Patch-DiT as a texture prompt. The texture prompt is introduced into each DiT block of Patch-DiT via a cross-attention mechanism [43], providing rich texture conditional guidance for the denoising process. Notably, our similarity-aware texture encoder is time-step independent, meaning that it does not need to be recalculated for each iteration, significantly accelerating inference process. As an efficient alternative, we introduce dimension-wise scaling parameters based on the time embedding in each cross-attention layer. Furthermore, by incorporating texture prompt, we mitigate the text-image misalignment issues typical in diffusion models with text prompt [7], which is particularly beneficial for SISR, as it ensures more consistent results in image super-resolution.

4. Experiments

4.1. Experimental Settings

Training Details. We train our PatchScaler based on the LSDIR [24] and HQ-50K [57] datasets, which consist of large-scale high-resolution images for image restoration. During training, the corresponding LR images are synthesized using the degradation pipeline of Real-ESRGAN [49]. The patch

size V is set to 16. We utilize the Adam optimizer [18] with a batch size of 6, and the learning rate is fixed as $5e-5$. Our PatchScaler is trained for 700K iterations using the Adam optimizer [18] with a batch size of 6, while GRM only participates in the training for the first 100K iterations based on Equation (1). The training process takes 10 days using eight NVIDIA Tesla V100 GPUs. More details about the network architecture are included in the supplementary material.

Inference Details. We evaluate our PatchScaler on both synthetic and real-world datasets. For synthetic data, we generate LR-HR pairs based on randomly selected 2000 test images from LSDIR [24], referred to as LSDIR-Test, following the degradation method used in ResShift [62]. We also evaluate our model on two real-world datasets: RealSR [6] and RealSet110. As the degradation in RealSR is monotonic and lacks common SR scenes such as animals and illustrations, we collect an extended dataset named RealSet110. It is worth noting that 98 of the LR images were collected from previous works [3, 15, 26, 29, 57, 62, 63], with the remaining images were collected from online sources. To evaluate the performance of our PatchScaler at both patch and image scales, the resolution of the LR images in LSDIR-Test and RealSR datasets is fixed at 128×128 , while the images in RealSet110 dataset have arbitrary resolutions. We classify the patches into three groups—"simple", "medium", and "hard"—following previous work [19, 46, 51], and argue that increasing the number of groups would make the differences between patches with different levels of reconstruction difficulty less obvious and increase the inference complexity of the model. Furthermore, to eliminate potential boundary effects within patches, we decompose the coarse HR feature into overlapping patches, which is commonly used in leading diffusion-based methods [2, 45]. We also apply wavelet-based color normalization [45] on the super-resolved image to align its low-frequency features with those of the LR input.

4.2. Comparisons with State-of-the-Art Methods

To verify the effectiveness of our PatchScaler, we conduct a series of quantitative and qualitative experiments with the following state-of-the-art SR methods: (1) classic CNN-based and Transformer-based SR methods: RealSR-JPEG [13], BSRGAN [63], RealESRGAN [49], and SwinIR [25]; (2) representative diffusion-based multi-step SR methods: LDM [38], StableSR [45], ResShift [62], DiffBIR [26], and PASD [59]; (3) the latest diffusion-based one-step SR methods: SinSR [50] and OSediff [52]. Following the default settings, the sampling step of ResShift [62] is set to 15. For other multi-step diffusion-based SR methods, it is set to 20. Moreover, we further analyze the performance of SUPIR [60] and PatchScaler in the supplementary material.

Evaluations on Synthetic Data. We first evaluate our PatchScaler on the synthetic LSDIR-TEST dataset. The quanti-

Table 1. Quantitative comparison with state-of-the-art SR methods on both synthetic and real-world datasets. The best and second best results are **highlighted** and underlined, respectively. PSNR/SSIM on Y channel are reported on each dataset. We calculate ManIQA metric based on the official ManIQA-KONIQ pre-trained model.

Methods	LSDIR-TEST						RealSR			RealSet110		
	PSNR	SSIM	LPIPS	ManIQA	CLIQQA	MUSIQ	ManIQA	CLIQQA	MUSIQ	ManIQA	CLIQQA	MUSIQ
RealSR-JPEG [13]	22.09	0.4819	0.3982	0.3647	0.6466	62.47	0.1710	0.5267	33.69	0.3030	0.7588	54.03
BSRGAN [63]	23.74	<u>0.5748</u>	0.3336	0.4069	0.6853	69.09	0.3787	0.5512	63.20	0.3870	0.7918	67.13
Real-ESRGAN [49]	23.08	0.5758	0.3234	0.4335	0.6810	69.91	0.3811	0.5492	60.56	0.3779	0.7844	65.05
SwinIR-GAN [25]	23.05	0.5698	0.3262	0.4195	0.6833	68.72	0.3583	0.5669	59.23	0.3598	<u>0.8009</u>	63.92
LDM [38]	24.14	0.5630	0.3323	0.3466	0.6735	61.83	0.2631	0.5617	47.72	0.2834	0.7628	55.01
StableSR [45]	23.09	0.5664	0.3170	0.4772	0.6739	69.91	0.3992	0.5350	61.33	0.3856	0.7851	62.08
ResShift [62]	<u>23.75</u>	0.5686	0.3102	0.5141	0.6919	69.62	0.3821	0.5694	58.81	0.4011	0.7584	62.07
PASD [59]	21.02	0.4940	0.3651	0.5177	0.6847	71.91	0.4656	0.5607	67.44	0.4378	0.7608	66.03
DiffBIR [26]	23.33	0.5305	0.3469	<u>0.5406</u>	0.6726	69.78	0.4546	0.5762	62.75	<u>0.4933</u>	0.7756	66.75
SinSR [50]	23.52	0.5577	0.3170	0.4866	0.6960	69.73	0.3998	0.5770	60.75	0.4250	0.6738	55.24
OSDiff [52]	22.50	0.5357	<u>0.3103</u>	0.4684	0.7070	72.16	<u>0.4744</u>	0.5890	<u>69.12</u>	0.4679	0.7949	<u>70.26</u>
PatchScaler	22.60	0.5297	0.3520	0.6261	0.7145	73.23	0.5225	<u>0.5839</u>	69.50	0.5442	0.8213	70.97

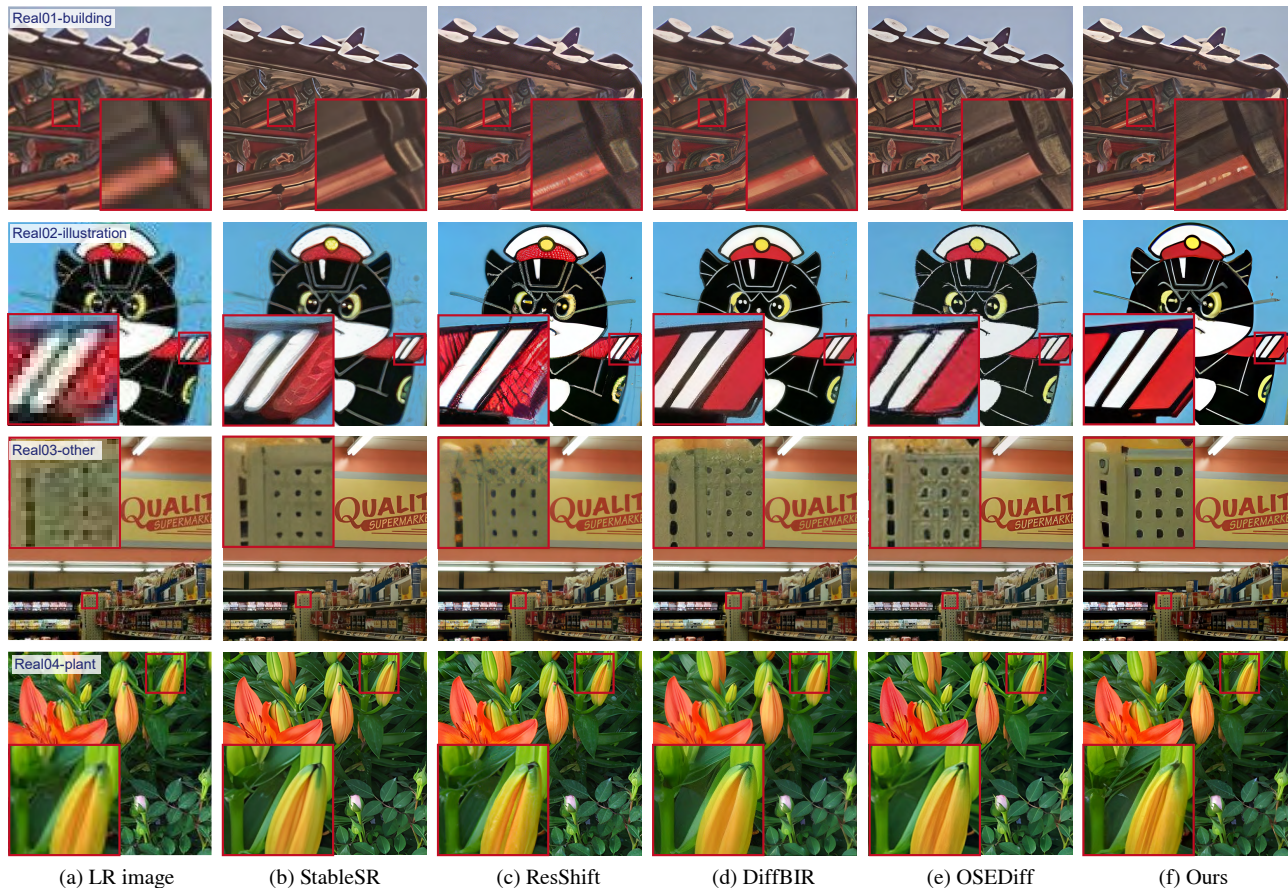


Figure 5. Visual comparisons of state-of-the-art SR methods on real-world low-resolution images.

tative results are presented in Table 1. It can be seen that our method outperforms all others in the non-reference metrics, i.e., ManIQA [58], CLIQQA [44] and MUSIQ [17]. ManIQA [58] utilizes a multi-dimensional attention network for perceptual assessment, CLIQQA [44] leverages rich visual language priors from CLIP to evaluate both the perceptual quality and perceptual abstraction, and MUSIQ [17] captures image quality at different granularities using a multi-

scale image quality Transformer. The consistent improvements across these metrics highlight PatchScaler’s superior ability to restore fine texture detail and achieve high perceptual quality. In addition, the full-reference metrics (i.e., PSNR, SSIM, and LPIPS [64]) are also given in Table 1 as a reference. However, it should be noted that these metrics only reflect certain aspects of performance and are poorly respond to realistic visuals[4, 11, 14, 20, 60], which can-

Table 2. Running time comparisons of the proposed PatchScaler to other methods on the $\times 4$ (512 \rightarrow 2048) SR task. The results are evaluated using an NVIDIA Tesla A100 GPU. Note that SinSR [50] suffers from an out-of-memory problem at this scale. The **highlighted** result is evaluated using dual-GPU parallel computing.

Methods	SwinIR-GAN [25]	LDM [38]	StableSR [45]	ResShift [62]	DiffBIR [26]	PASD [59]	SinSR [50]	OSDiff [52]	PatchScaler
Runtime (s)	1.55	25.82	35.22	14.89	78.12	59.03	-	30.35	3.41 (2.26)

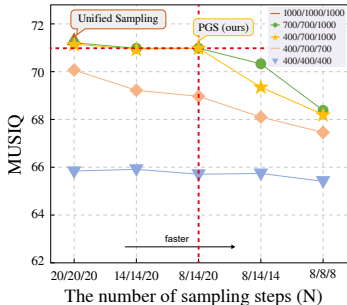


Figure 6. Performance analysis of PatchScaler on RealSet110 dataset under different configurations. Our PatchScaler achieves a better tradeoff between metrics and runtime at the intersection of two red dashed lines.

not reliably evaluate the performance of diffusion-based SR models. As the generative capabilities of models improve, it becomes increasingly necessary to reexamine these full-reference metrics and consider more effective evaluation methods for diffusion-based SR models.

Evaluations on Real-World Data. As shown in Table 1, we further evaluate PatchScaler on two real-world datasets. It can be seen that our method surpasses others in both ManIQA [58] and MUSIQ [17] metrics, indicating the excellent performance of our approach. Moreover, PatchScaler also demonstrates competitive performance in CLIPQA [44] metric, with an improvement of **+0.0204** over the second-best results on the RealSet110 dataset. We also provide qualitative comparisons with other diffusion-based SR methods on four LR images in Figure 5. It can be observed that other diffusion-based SR methods struggle to reconstruct realistic textures. StableSR [45] tends to produce highly blurred (e.g., Real02-illustration) results with unclear texture details. The results of ResShift [62] and DiffBIR [26] contain inaccurate generation, which negatively impacts visual perception. In addition, OSDiff [52] employs a uniform one-step strategy to minimize sampling steps indiscriminately across all image regions, resulting in unsatisfactory reconstruction results in regions with complex textures (e.g., Real03-other). In contrast, our PatchScaler succeeds in producing realistic results at both the patch and global levels, with much better perceptual quality and richer fine-details. More visual comparisons can be found in the supplementary material.

Efficiency Evaluations. To assess the efficiency of PatchScaler, we compare its runtime against other diffusion-based SR methods on the $\times 4$ (512 \rightarrow 2048) SR task, as shown in Table 2. We also provide the runtime of the traditional transformer-based method SwinIR-GAN [25] as a reference. Due to the lack of optimization for high-resolution inputs, the inference time of OSDiff [52] is quite long. Moreover, SinSR [50] suffers from an out-of-memory problem at this scale. In contrast, PatchScaler achieves the fastest inference

time among the diffusion-based methods, just **0.23** \times that of the second fastest ResShift [62]. The efficiency gains of PatchScaler can be attributed to two main factors. First, the denoising process in PatchScaler is performed at the patch level, reducing the computational load on the self-attention mechanism across the entire image. Second, the PGS treats different image regions discriminatively and dynamically assigns sampling configurations for different patches, providing an efficient inference process, especially for high-resolution images. In addition, we highlight that PGS also allows the use of multiple GPUs to process patches from different groups separately. To demonstrate this, we re-evaluate our PatchScaler using two NVIDIA Tesla A100 GPUs. By assigning one GPU to handle patches from the hard group and another to handle patches from the simple and medium groups, our PatchScaler achieves an additional **33.7%** inference speedup over the single-GPU setting, showcasing the scalability of our PatchScaler in parallel computing.

4.3. Evaluations of Patch-adaptive Group Sampling

A key feature of PatchScaler is the proposed PGS, which accelerates inference by introducing adaptive sampling for different patches. Here, we conduct a series of experiments to analyze the performance of PatchScaler under different configurations and to further validate the extension of PGS.

Determine Appropriate Configurations. Figure 6 provides an intuitive experiment analysis (metrics against runtime) of the performance of PatchScaler under different configurations. Specifically, it can be found that when reducing the intermediate time steps T_1 , T_2 , and T_3 of simple, medium, and hard patches from [1000, 1000, 1000] to [400, 700, 1000], PatchScaler consistently achieves competitive performance. This is because simple patches have higher confidence and a smaller distance Δx_0 to the ground truth, allowing a larger $\sqrt{\alpha_\tau}$ (i.e., a smaller τ) to satisfy Equation (6), and vice versa. However, further reducing these time steps significantly deteriorates performance, indicating that small intermediate time steps fail to satisfy Equation (6). Thus, we set $\tau_1=400$, $\tau_2=700$, and $\tau_3=1000$ to achieve an adaptive shortcut path for each group. With this configuration, we continue to explore different settings for the sampling step N . It can be observed that by reducing the number of iterations N_1 , N_2 and N_3 from [20, 20, 20] to [8, 14, 20], the performance of the model can be well maintained. This is understandable since a large number of sampling steps is redundant for a small τ . However, further reducing the number of sampling steps significantly decreases the performance scores of the

Table 3. Quantitative comparison of StableSR and StableSR+PGS. The best results are **highlighted**. The runtime is measured on the $\times 4$ (512 \rightarrow 2048) SR task using an NVIDIA Tesla A100 GPU.

Methods	ManIQA	CLIQQA	MUSIQ	Runtime (s)
StableSR	0.3856	0.7851	62.08	35.22
StableSR+PGS	0.5035	0.7809	65.54	8.53

Table 4. Ablation studies of different prompt in our method. The best results are **highlighted**.

Prompt type	ManIQA	CLIQQA	MUSIQ
Text prompt	0.4849	0.7890	66.79
Texture prompt	0.5442	0.8213	70.97

three metrics. Consequently, there is a trade-off between the sampling step N and the performance on the setting of $N_1=8$, $N_2=14$, and $N_3=20$. By discriminatively assigning sampling steps to each group, PatchScaler achieves an adaptive sampling process with fewer total steps than unified sampling, resulting in a significant speedup the inference process. In addition, to better distinguish patches of varying difficulty, we set γ_1 and γ_2 to 0.95 and 0.75, respectively, in practice. More ablation studies can be found in the supplementary material. We present the examples of coarse HR images and corresponding quantified confidence maps Q_{map} in Figure 4. It can be seen that this setting can accurately quantify the reconstruction difficulty of different regions.

The Extension of PGS. Since PGS is not involved in model training, it can be seamlessly extended to other architectures and tasks as a plug-and-play component and achieve dynamic acceleration of model inference. As an example, we applied the proposed PGS and GRM to StableSR [45] in a trainable-free manner. Since its backbone, Stable Diffusion [38], performs best with a latent feature size of 64, we set the patch size V to 64. The quantitative and qualitative results are presented in Table 3 and Figure 7, which show that our PGS achieves significant improvements in both quantitative metrics (ManIQA: **+0.1179**; MUSIQ: **+3.46**) and qualitative comparisons, and further accelerates the model inference efficiency (only **0.24** \times) of StableSR. This reveals that adopting a unified sampling strategy is suboptimal and redundant. In contrast, by dynamically assigning sampling configurations to different patches, our PGS can significantly accelerate the inference process of existing diffusion-based models, While maintaining reconstruction quality.

4.4. Text Prompt vs. Texture Prompt

To further improve the denoising capability at each step of model inference, we introduce a texture prompt for PatchDiT, which mitigates the text-image misalignment problem associated with text prompt and provides rich conditional information by retrieving high-quality and patch-independent texture priors from a reference texture memory. In this section, we conduct ablation studies between text prompt and



Figure 7. Visual comparison between StableSR and StableSR+PGS. Our method can be easily extended to other baselines and can significantly improve the reconstruction quality.

texture prompt on the RealSet110 dataset. Since HR images are not available during inference, we utilize the BLIP-2 vision-language pre-training model [22] to generate the text information from the LR image, and then obtain the text prompt based on the CLIP model [37]. The results are presented in Table 4. It can be seen that the model with a texture prompt achieves higher scores in three quantitative metrics than the model with a text prompt. This is due to the challenging misalignment [7] between the text content and image content in the SISR task, which often leads to degraded performance. We discuss this misalignment problem further in the supplementary material by analyzing the performance of SUPIR [60] and PatchScaler. These conclusions demonstrate the effectiveness of the proposed texture prompt in improving the performance of PatchScaler.

4.5. Discussion

Since the unified sampling process with a large number of steps is applied indiscriminately to different image regions, the existing diffusion-based multi-step SR methods (e.g., DiffBIR [26], PASD [59], and SUPIR [60]) require expensive computational costs. This restricts their applicability to a few non-time-sensitive post-processing scenarios. Although real-time performance remains unresolved for all diffusion-based SR methods, our PatchScaler shows a significant improvement in computational efficiency while maintaining reconstruction quality, particularly when dealing with high-resolution images. In the quantitative evaluation of Table 2, the runtime of PatchScaler outperforms diffusion-based one-step SR methods and rivals state-of-the-art GAN-based models (e.g. SwinIR-GAN [25]). This presents exciting opportunities for a wide range of users, including researchers, photographers, and technology companies. In the future, we will explore integration options with existing sampling distillation solutions and further improve the deployment efficiency through engineering solutions.

5. Conclusion

In this paper, we have presented PatchScaler, an efficient patch-independent diffusion-based SR model. It is motivated by the observation that performing the unified sampling equally on different images regions is redundant. We devel-

oped a PGS strategy to discriminatively assign an appropriate sampling configuration for each patch according to a quantified confidence map so that the high-resolution images can be efficiently recovered. Additionally, we introduced a texture prompt for Patch-DiT to provide rich texture condition information by retrieving high-quality patch-independent texture priors from a reference texture memory. Our PatchScaler can efficiently solve SISR problem and achieve superior performance both quantitatively and qualitatively.

References

- [1] Eirikur Agustsson and Radu Timofte. Ntire 2017 challenge on single image super-resolution: Dataset and study. In *Proceedings of the IEEE conference on computer vision and pattern recognition workshops*, pages 126–135, 2017. 5
- [2] Omer Bar-Tal, Lior Yariv, Yaron Lipman, and Tali Dekel. Multidiffusion: Fusing diffusion paths for controlled image generation. 2023. 5
- [3] Sean Bell, Paul Upchurch, Noah Snaveley, and Kavita Bala. Material recognition in the wild with the materials in context database. In *Proceedings of the IEEE conference on computer vision and pattern recognition*, pages 3479–3487, 2015. 5
- [4] Yochai Blau and Tomer Michaeli. The perception-distortion tradeoff. In *Proceedings of the IEEE conference on computer vision and pattern recognition*, pages 6228–6237, 2018. 6
- [5] Tim Brooks, Aleksander Holynski, and Alexei A Efros. Instructpix2pix: Learning to follow image editing instructions. In *Proceedings of the IEEE/CVF Conference on Computer Vision and Pattern Recognition*, pages 18392–18402, 2023. 1
- [6] Jianrui Cai, Hui Zeng, Hongwei Yong, Zisheng Cao, and Lei Zhang. Toward real-world single image super-resolution: A new benchmark and a new model. In *Proceedings of the IEEE/CVF international conference on computer vision*, pages 3086–3095, 2019. 1, 5
- [7] Junsong Chen, Jincheng Yu, Chongjian Ge, Lewei Yao, Enze Xie, Yue Wu, Zhongdao Wang, James Kwok, Ping Luo, Huchuan Lu, et al. Pixart- α : Fast training of diffusion transformer for photorealistic text-to-image synthesis. *arXiv preprint arXiv:2310.00426*, 2023. 2, 5, 8
- [8] Mircea Cimpoi, Subhansu Maji, Iasonas Kokkinos, Sammy Mohamed, and Andrea Vedaldi. Describing textures in the wild. In *Proceedings of the IEEE conference on computer vision and pattern recognition*, pages 3606–3613, 2014.
- [9] Prafulla Dhariwal and Alexander Nichol. Diffusion models beat gans on image synthesis. *Advances in neural information processing systems*, 34:8780–8794, 2021. 1
- [10] Ian Goodfellow, Jean Pouget-Abadie, Mehdi Mirza, Bing Xu, David Warde-Farley, Sherjil Ozair, Aaron Courville, and Yoshua Bengio. Generative adversarial networks. *Communications of the ACM*, 63(11):139–144, 2020. 2
- [11] Jinjin Gu, Haoming Cai, Chao Dong, Jimmy S Ren, Radu Timofte, Yuan Gong, Shanshan Lao, Shuwei Shi, Jiahao Wang, Sidi Yang, et al. Ntire 2022 challenge on perceptual image quality assessment. In *Proceedings of the IEEE/CVF conference on computer vision and pattern recognition*, pages 951–967, 2022. 6
- [12] Jonathan Ho, Ajay Jain, and Pieter Abbeel. Denoising diffusion probabilistic models. *Advances in neural information processing systems*, 33:6840–6851, 2020. 1, 3
- [13] Xiaozhong Ji, Yun Cao, Ying Tai, Chengjie Wang, Jilin Li, and Feiyue Huang. Real-world super-resolution via kernel estimation and noise injection. In *proceedings of the IEEE/CVF conference on computer vision and pattern recognition workshops*, pages 466–467, 2020. 2, 5, 6
- [14] Gu Jinjin, Cai Haoming, Chen Haoyu, Ye Xiaoxing, Jimmy S Ren, and Dong Chao. PIPal: a large-scale image quality assessment dataset for perceptual image restoration. In *Computer Vision—ECCV 2020: 16th European Conference, Glasgow, UK, August 23–28, 2020, Proceedings, Part XI 16*, pages 633–651. Springer, 2020. 6
- [15] Tero Karras, Samuli Laine, and Timo Aila. A style-based generator architecture for generative adversarial networks. In *Proceedings of the IEEE/CVF conference on computer vision and pattern recognition*, pages 4401–4410, 2019. 5
- [16] Bahjat Kawar, Shiran Zada, Oran Lang, Omer Tov, Huiwen Chang, Tali Dekel, Inbar Mosseri, and Michal Irani. Imagic: Text-based real image editing with diffusion models. In *Proceedings of the IEEE/CVF Conference on Computer Vision and Pattern Recognition*, pages 6007–6017, 2023. 1
- [17] Junjie Ke, Qifei Wang, Yilin Wang, Peyman Milanfar, and Feng Yang. Musiq: Multi-scale image quality transformer. In *Proceedings of the IEEE/CVF international conference on computer vision*, pages 5148–5157, 2021. 6, 7
- [18] Diederik P Kingma and Jimmy Ba. Adam: A method for stochastic optimization. *arXiv preprint arXiv:1412.6980*, 2014. 5
- [19] Xiangtao Kong, Hengyuan Zhao, Yu Qiao, and Chao Dong. Classsr: A general framework to accelerate super-resolution networks by data characteristic. In *Proceedings of the IEEE/CVF conference on computer vision and pattern recognition*, pages 12016–12025, 2021. 5
- [20] Christian Ledig, Lucas Theis, Ferenc Huszár, Jose Caballero, Andrew Cunningham, Alejandro Acosta, Andrew Aitken, Alykhan Tejani, Johannes Totz, Zehan Wang, et al. Photo-realistic single image super-resolution using a generative adversarial network. In *Proceedings of the IEEE conference on computer vision and pattern recognition*, pages 4681–4690, 2017. 6
- [21] Juncheng Li, Faming Fang, Kangfu Mei, and Guixu Zhang. Multi-scale residual network for image super-resolution. In *Proceedings of the European conference on computer vision (ECCV)*, pages 517–532, 2018. 2
- [22] Junnan Li, Dongxu Li, Silvio Savarese, and Steven Hoi. Blip-2: Bootstrapping language-image pre-training with frozen image encoders and large language models. In *International conference on machine learning*, pages 19730–19742. PMLR, 2023. 8
- [23] Wenbo Li, Kun Zhou, Lu Qi, Nianjuan Jiang, Jiangbo Lu, and Jiaya Jia. Lapar: Linearly-assembled pixel-adaptive regression network for single image super-resolution and beyond. *Advances in Neural Information Processing Systems*, 33:20343–20355, 2020. 1
- [24] Yawei Li, Kai Zhang, Jingyun Liang, Jiezhang Cao, Ce Liu, Rui Gong, Yulun Zhang, Hao Tang, Yun Liu, Denis Deman-

- dolx, et al. Lsdnr: A large scale dataset for image restoration. In *Proceedings of the IEEE/CVF Conference on Computer Vision and Pattern Recognition*, pages 1775–1787, 2023. 5
- [25] Jingyun Liang, Jiezhong Cao, Guolei Sun, Kai Zhang, Luc Van Gool, and Radu Timofte. Swinir: Image restoration using swin transformer. In *Proceedings of the IEEE/CVF international conference on computer vision*, pages 1833–1844, 2021. 1, 2, 5, 6, 7, 8
- [26] Xinqi Lin, Jingwen He, Ziyang Chen, Zhaoyang Lyu, Ben Fei, Bo Dai, Wanli Ouyang, Yu Qiao, and Chao Dong. Diffbir: Towards blind image restoration with generative diffusion prior. *arXiv preprint arXiv:2308.15070*, 2023. 1, 2, 5, 6, 7, 8
- [27] Yong Liu, Hang Dong, Boyang Liang, Songwei Liu, Qingji Dong, Kai Chen, Fangmin Chen, Lean Fu, and Fei Wang. Unfolding once is enough: A deployment-friendly transformer unit for super-resolution. In *Proceedings of the 31st ACM International Conference on Multimedia*, pages 7952–7960, 2023. 1, 2
- [28] Ze Liu, Yutong Lin, Yue Cao, Han Hu, Yixuan Wei, Zheng Zhang, Stephen Lin, and Baining Guo. Swin transformer: Hierarchical vision transformer using shifted windows. In *Proceedings of the IEEE/CVF international conference on computer vision*, pages 10012–10022, 2021. 2
- [29] Andreas Lugmayr, Martin Danelljan, and Radu Timofte. Ntire 2020 challenge on real-world image super-resolution: Methods and results. In *Proceedings of the IEEE/CVF Conference on Computer Vision and Pattern Recognition Workshops*, pages 494–495, 2020. 5
- [30] Yusuke Matsui, Kota Ito, Yuji Aramaki, Azuma Fujimoto, Toru Ogawa, Toshihiko Yamasaki, and Kiyoharu Aizawa. Sketch-based manga retrieval using manga109 dataset. *Multimedia tools and applications*, 76:21811–21838, 2017. 5
- [31] Kangfu Mei, Mauricio Delbracio, Hossein Talebi, Zhengzhong Tu, Vishal M Patel, and Peyman Milanfar. Conditional diffusion distillation. *arXiv preprint arXiv:2310.01407*, 2023. 1
- [32] Chenlin Meng, Robin Rombach, Ruiqi Gao, Diederik Kingma, Stefano Ermon, Jonathan Ho, and Tim Salimans. On distillation of guided diffusion models. In *Proceedings of the IEEE/CVF Conference on Computer Vision and Pattern Recognition*, pages 14297–14306, 2023. 3
- [33] Qian Ning, Weisheng Dong, Xin Li, Jinjian Wu, and Guangming Shi. Uncertainty-driven loss for single image super-resolution. *Advances in Neural Information Processing Systems*, 34:16398–16409, 2021. 2
- [34] William Peebles and Saining Xie. Scalable diffusion models with transformers. In *Proceedings of the IEEE/CVF International Conference on Computer Vision*, pages 4195–4205, 2023. 3
- [35] Charles R Qi, Hao Su, Kaichun Mo, and Leonidas J Guibas. Pointnet: Deep learning on point sets for 3d classification and segmentation. In *Proceedings of the IEEE conference on computer vision and pattern recognition*, pages 652–660, 2017. 5
- [36] Rui Qin, Ming Sun, Fangyuan Zhang, Xing Wen, and Bin Wang. Blind image super-resolution with rich texture-aware codebook. In *Proceedings of the 31st ACM International Conference on Multimedia*, pages 676–687, 2023. 4
- [37] Alec Radford, Jong Wook Kim, Chris Hallacy, Aditya Ramesh, Gabriel Goh, Sandhini Agarwal, Girish Sastry, Amanda Askell, Pamela Mishkin, Jack Clark, et al. Learning transferable visual models from natural language supervision. In *International conference on machine learning*, pages 8748–8763. PMLR, 2021. 8
- [38] Robin Rombach, Andreas Blattmann, Dominik Lorenz, Patrick Esser, and Björn Ommer. High-resolution image synthesis with latent diffusion models. In *Proceedings of the IEEE/CVF conference on computer vision and pattern recognition*, pages 10684–10695, 2022. 1, 3, 5, 6, 7, 8
- [39] Nataniel Ruiz, Yuanzhen Li, Varun Jampani, Yael Pritch, Michael Rubinstein, and Kfir Aberman. Dreambooth: Fine tuning text-to-image diffusion models for subject-driven generation. In *Proceedings of the IEEE/CVF Conference on Computer Vision and Pattern Recognition*, pages 22500–22510, 2023. 3
- [40] Edgar Schonfeld, Bernt Schiele, and Anna Khoreva. A u-net based discriminator for generative adversarial networks. In *Proceedings of the IEEE/CVF conference on computer vision and pattern recognition*, pages 8207–8216, 2020. 2
- [41] Jascha Sohl-Dickstein, Eric Weiss, Niru Maheswaranathan, and Surya Ganguli. Deep unsupervised learning using nonequilibrium thermodynamics. In *International conference on machine learning*, pages 2256–2265. PMLR, 2015. 1, 3
- [42] Long Sun, Jinshan Pan, and Jinhui Tang. Shufflemixer: An efficient convnet for image super-resolution. *Advances in Neural Information Processing Systems*, 35:17314–17326, 2022. 2
- [43] Ashish Vaswani, Noam Shazeer, Niki Parmar, Jakob Uszkoreit, Llion Jones, Aidan N Gomez, Łukasz Kaiser, and Illia Polosukhin. Attention is all you need. *Advances in neural information processing systems*, 30, 2017. 5
- [44] Jianyi Wang, Kelvin CK Chan, and Chen Change Loy. Exploring clip for assessing the look and feel of images. In *Proceedings of the AAAI Conference on Artificial Intelligence*, pages 2555–2563, 2023. 6, 7
- [45] Jianyi Wang, Zongsheng Yue, Shangchen Zhou, Kelvin CK Chan, and Chen Change Loy. Exploiting diffusion prior for real-world image super-resolution. *International Journal of Computer Vision*, pages 1–21, 2024. 1, 2, 5, 6, 7, 8
- [46] Qi Wang, Weiwei Fang, Meng Wang, and Yusong Cheng. Classification-based dynamic network for efficient super-resolution. In *ICASSP 2023-2023 IEEE International Conference on Acoustics, Speech and Signal Processing (ICASSP)*, pages 1–5. IEEE, 2023. 5
- [47] Xintao Wang, Ke Yu, Chao Dong, and Chen Change Loy. Recovering realistic texture in image super-resolution by deep spatial feature transform. In *Proceedings of the IEEE conference on computer vision and pattern recognition*, pages 606–615, 2018. 5
- [48] Xintao Wang, Ke Yu, Shixiang Wu, Jinjin Gu, Yihao Liu, Chao Dong, Yu Qiao, and Chen Change Loy. ESRGAN: Enhanced super-resolution generative adversarial networks. In *Proceedings of the European conference on computer vision (ECCV) workshops*, pages 0–0, 2018. 2

- [49] Xintao Wang, Liangbin Xie, Chao Dong, and Ying Shan. Real-esrgan: Training real-world blind super-resolution with pure synthetic data. In *Proceedings of the IEEE/CVF international conference on computer vision*, pages 1905–1914, 2021. 1, 2, 5, 6
- [50] Yufei Wang, Wenhan Yang, Xinyuan Chen, Yaohui Wang, Lanqing Guo, Lap-Pui Chau, Ziwei Liu, Yu Qiao, Alex C Kot, and Bihan Wen. Sinsr: Diffusion-based image super-resolution in a single step. *arXiv preprint arXiv:2311.14760*, 2023. 1, 5, 6, 7
- [51] Yan Wang, Shijie Zhao, Yi Liu, Junlin Li, and Li Zhang. Camixersr: Only details need more" attention". *arXiv preprint arXiv:2402.19289*, 2024. 5
- [52] Rongyuan Wu, Lingchen Sun, Zhiyuan Ma, and Lei Zhang. One-step effective diffusion network for real-world image super-resolution. *arXiv preprint arXiv:2406.08177*, 2024. 5, 6, 7
- [53] Xu Yan, Weibing Zhao, Kun Yuan, Ruimao Zhang, Zhen Li, and Shuguang Cui. Towards content-independent multi-reference super-resolution: Adaptive pattern matching and feature aggregation. In *Computer Vision—ECCV 2020: 16th European Conference, Glasgow, UK, August 23–28, 2020, Proceedings, Part XXV 16*, pages 52–68. Springer, 2020. 4
- [54] Fei Yang, Shiqi Yang, Muhammad Atif Butt, Joost van de Weijer, et al. Dynamic prompt learning: Addressing cross-attention leakage for text-based image editing. *Advances in Neural Information Processing Systems*, 36, 2024. 1
- [55] Jingyu Yang, Sheng Shen, Huanjing Yue, and Kun Li. Implicit transformer network for screen content image continuous super-resolution. *Advances in Neural Information Processing Systems*, 34:13304–13315, 2021. 1
- [56] Ling Yang, Jingwei Liu, Shenda Hong, Zhilong Zhang, Zhilin Huang, Zheming Cai, Wentao Zhang, and Bin Cui. Improving diffusion-based image synthesis with context prediction. *Advances in Neural Information Processing Systems*, 36, 2024. 1
- [57] Qinhong Yang, Dongdong Chen, Zhentao Tan, Qiankun Liu, Qi Chu, Jianmin Bao, Lu Yuan, Gang Hua, and Nenghai Yu. Hq-50k: A large-scale, high-quality dataset for image restoration. *arXiv preprint arXiv:2306.05390*, 2023. 5
- [58] Sidi Yang, Tianhe Wu, Shuwei Shi, Shanshan Lao, Yuan Gong, Mingdeng Cao, Jiahao Wang, and Yujiu Yang. Maniqa: Multi-dimension attention network for no-reference image quality assessment. In *Proceedings of the IEEE/CVF Conference on Computer Vision and Pattern Recognition*, pages 1191–1200, 2022. 6, 7
- [59] Tao Yang, Rongyuan Wu, Peiran Ren, Xuansong Xie, and Lei Zhang. Pixel-aware stable diffusion for realistic image super-resolution and personalized stylization. *arXiv preprint arXiv:2308.14469*, 2023. 1, 5, 6, 7, 8
- [60] Fanghua Yu, Jinjin Gu, Zheyuan Li, Jinfan Hu, Xiangtao Kong, Xintao Wang, Jingwen He, Yu Qiao, and Chao Dong. Scaling up to excellence: Practicing model scaling for photo-realistic image restoration in the wild, 2024. 5, 6, 8
- [61] Zongsheng Yue, Jianyi Wang, and Chen Change Loy. Efficient diffusion model for image restoration by residual shifting. *arXiv preprint arXiv:2403.07319*, 2024. 1
- [62] Zongsheng Yue, Jianyi Wang, and Chen Change Loy. Resshift: Efficient diffusion model for image super-resolution by residual shifting. *Advances in Neural Information Processing Systems*, 36, 2024. 1, 2, 5, 6, 7
- [63] Kai Zhang, Jingyun Liang, Luc Van Gool, and Radu Timofte. Designing a practical degradation model for deep blind image super-resolution. In *Proceedings of the IEEE/CVF International Conference on Computer Vision*, pages 4791–4800, 2021. 2, 5, 6
- [64] Richard Zhang, Phillip Isola, Alexei A Efros, Eli Shechtman, and Oliver Wang. The unreasonable effectiveness of deep features as a perceptual metric. In *Proceedings of the IEEE conference on computer vision and pattern recognition*, pages 586–595, 2018. 6
- [65] Wenlong Zhang, Xiaohui Li, Guangyuan Shi, Xiangyu Chen, Yu Qiao, Xiaoyun Zhang, Xiao-Ming Wu, and Chao Dong. Real-world image super-resolution as multi-task learning. *Advances in Neural Information Processing Systems*, 36, 2024. 1
- [66] Xindong Zhang, Hui Zeng, Shi Guo, and Lei Zhang. Efficient long-range attention network for image super-resolution. In *European conference on computer vision*, pages 649–667. Springer, 2022. 1
- [67] Zhifei Zhang, Zhaowen Wang, Zhe Lin, and Hairong Qi. Image super-resolution by neural texture transfer. In *Proceedings of the IEEE/CVF conference on computer vision and pattern recognition*, pages 7982–7991, 2019. 4, 5
- [68] Qingping Zheng, Yuanfan Guo, Jiankang Deng, Jianhua Han, Ying Li, Songcen Xu, and Hang Xu. Any-size-diffusion: Toward efficient text-driven synthesis for any-size hd images. In *Proceedings of the AAAI Conference on Artificial Intelligence*, pages 7571–7578, 2024. 3
- [69] Shangchen Zhou, Jiawei Zhang, Wangmeng Zuo, and Chen Change Loy. Cross-scale internal graph neural network for image super-resolution. *Advances in neural information processing systems*, 33:3499–3509, 2020. 1, 2